Available online at www.sciencedirect.com
SCIENCE DIRECT®
Journal of Solid State Chemistry 177 (2004) 1493–1500
JOURNAL OF SOLID STATE CHEMISTRY
http://elsevier.com/locate/jssc

Crystal growth of new perovskite and perovskite related iridates: $Ba_3LiIr_2O_9$, $Ba_3NaIr_2O_9$, and $Ba_{3.44}K_{1.56}Ir_2O_{10}$

Seung-Joo Kim,[a] Mark D. Smith,[a] Jacques Darriet,[b] and Hans-Conrad zur Loye[a,*]

[a] *Department of Chemistry & Biochemistry, University of South Carolina, 631 Sumter St. Columbia, SC 29208, USA*
[b] *Institut de Chimie de la Matière Condensée de Bordeaux (ICMCB-CNRS), Avenue du Dr. Schweitzer, 33608 Pessac Cedex, France*

Received 9 October 2003; accepted 26 November 2003

Abstract

Single crystals of $Ba_3LiIr_2O_9$, $Ba_3NaIr_2O_9$, and $Ba_{3.44}K_{1.56}Ir_2O_{10}$ were grown from hydroxide fluxes. $Ba_3LiIr_2O_9$ and $Ba_3NaIr_2O_9$ form in the 6H–$BaTiO_3$ or triple perovskite structure, which is derived from the hexagonal and cubic stacking of $[AO_3]$ layers. The structure contains face-sharing Ir_2O_9 octahedra pairs, which are connected via corner shared LiO_6 (NaO_6) octahedra. Both compounds crystallize in the space group $P6_3/mmc$, $Z = 2$, with $a = 5.7804(4)$ and $c = 14.302(1)$ and $a = 5.866(4)$ and $c = 14.596(1)$ for the Li and Na member, respectively. The structure of $Ba_{3.44}K_{1.56}Ir_2O_{10}$ is derived from the stacking of $[AO_3]$ and mixed $[A_2O]$ layers, and is an $n = 3$ member of the $[A_nM_{n-1}O_{3n}][A_2O]$ family of hexagonal perovskite related oxides. The structure of $Ba_{3.44}K_{1.56}Ir_2O_{10}$ consists of ($Ba_3Ir_2O_9$) slabs separated by $[(Ba,K)_2O]$ layers and is isostructural with $Ba_5Ru_2O_{10}$. The ($Ba_3Ir_2O_9$) slabs contain isolated, face-sharing Ir_2O_9 octahedra pairs. The compound crystallizes in the space group $P6_3/mmc$, $Z = 2$, with $a = 5.91330(1)$ Å and $c = 18.1792(7)$ Å. The magnetic moments determined from the temperature dependence of the magnetic susceptibility are low for all three oxides, which is thought to be due to a combination of spin–orbit coupling and strong exchange interactions within the iridium octahedra pairs.

Keywords: Oxides; Crystal growth; Magnetic properties; Crystal structure

1. Introduction

In the field of solid-state chemistry, the perovskite family of oxides is perhaps the most studied group of oxides known. What has generated and sustained interest in this fascinating family of oxides is the large and ever-surprising variety of properties exhibited, as well as the extensive compositional flexibility [1] that enables this structure to accommodate almost every element in the periodic table. Significant interest continues to focus on the structural variety exhibited by the perovskite family of compounds, where both the cubic and the hexagonal perovskite structure can be generated from the stacking of close packed $[AO_3]$ layers and the subsequent filling of the generated octahedral sites by the *B*-cation; an *ABC* type stacking results in the cubic and an *AB* stacking results in the hexagonal (2H) perovskite structure [2,3]. In addition to the cubic and hexagonal ABO_3 structures, there exist a variety of intergrowth structures that combine the *AB* and *ABC* stacking sequences, forming the 6H-triple perovskite, $A_3BB'_2O_9$, (such as $Ba_3LiIr_2O_9$ and $Ba_3NaIr_2O_9$ discussed in this paper) or the 8H-quadruple perovskite, $A_4BB'_3O_{12}$ [4–6]. Further structural variety in the extended perovskite family of oxides arises if one allows for the inclusion of modified layers within the stacking sequence. For example, the incorporation of $[A_3A'O_6]$ layers leads to the $A_{3n+3m}A'_nB_{3m+n}O_{9m+6n}$ family of structures that was first described by Darriet and Subramanian [7]. Likewise, the incorporation of $[A_2O]$ layers leads to new structure types that are perovskite related. Recently, an example of such a perovskite related structure, $Ba_5Ru_2O_{10}$, containing $[A_2O]$ layers, was reported and shown to be the $n = 3$ member of a family of phases described by the general formula $[A_nB_{n-1}O_{3n}][A_2O]$ [8]. $Ba_{3.44}K_{1.56}Ir_2O_{10}$, a new perovskite related oxide discussed in this paper, is isostructural with $Ba_5Ru_2O_{10}$ and is the first iridium containing $n = 3$ oxide belonging to this family.

*Corresponding author. Fax: 8037778508.
E-mail address: jssc@mail.chem.sc.edu (H.-C. zur Loye).

0022-4596/$ - see front matter © 2004 Elsevier Inc. All rights reserved.
doi:10.1016/j.jssc.2003.11.037

For the past 10 years, our group has explored the single crystal growth of perovskite related oxides from high temperature solutions [9–17]. This well-established method [18] is particularly applicable to oxides, as exemplified by the numerous published compositions containing elements from nearly every section of the periodic table in a wide range of oxidation states. Oxide crystals have been grown from a variety of different high temperature solutions, including alkali and alkaline earth carbonates, halides, peroxides, super oxides, and hydroxides [11,12,19–24]. Of all these diverse solvent systems, the hydroxide melts have proven to be particularly advantageous for obtaining single crystals containing elements in unusually high oxidation states, as exemplified by systems such as Ni(IV) in $Ba_6Ni_5O_{15}$ [25], Rh(V) in Sr_3NaRhO_6 [23], and Os(VII) in Ba_2NaOsO_6 [9].

Recently, we have explored iridium-containing oxides and established the reaction conditions by which high quality single crystals can be grown from high temperature solutions [11,12,26–30]. While there are numerous examples of perovskite related iridium oxides with oxidation states of Ir(IV) and Ir(V) [20,31–35], compounds containing Ir(VI) have until now only been prepared under very high oxygen pressure [36]. In this paper, we present three new iridium containing oxides, $Ba_3LiIr_2O_9$, $Ba_3NaIr_2O_9$, and $Ba_{3.44}K_{1.56}Ir_2O_{10}$, containing iridium in unusually high average oxidation states of 5.5, 5.5 and 5.78, respectively. The structures and magnetic properties are discussed.

2. Experimental

2.1. Crystal growth of $Ba_{3.44}K_{1.56}Ir_2O_{10}$

Ir powder (0.064 g, 0.33 mmol; Engelhard, 99.5%), $Ba(OH)_2$ (0.63 g, 2.0 mmol; obtained from the dehydration of $Ba(OH)_2 \cdot 8H_2O$ by heating at 250°C for 2 h), KO_2 (0.7 g, 10 mmol; Alfa, 96.5%) and KOH (4.0 g, 71 mmol; Fisher, ACS reagent) were placed in a 12.5 mm diameter silver tube that had been sealed at one end and which was crimped at the other end. The silver tube was placed into a box furnace and heated to the reaction temperature of 700°C at 50°C/h, held for 10 h, and then slowly cooled to 400°C at 10°C/h followed by cooling to room temperature by turning off the furnace. The crystals were extracted from the flux matrix by sonication in methanol and then stored in a vacuum desiccator.

2.2. Crystal growth of $Ba_3LiIr_2O_9$ and $Ba_3NaIr_2O_9$

$Ba_3LiIr_2O_9$:Ir powder (0.1922 g, 1.0 mmol; Engelhard, 99.5%), $Ba(OH)_2 \cdot 8H_2O$ (0.47 g, 1.5 mmol; Fisher, ACS reagent), KOH (2.82 g, 50 mmol; Fisher, ACS reagent) and $LiOH \cdot H_2O$ (0.084 g, 2 mmol; Fisher, ACS reagent); $Ba_3NaIr_2O_9$:Ir powder (Engelhard, 99.5%) (0.096 g, 0.5 mmol), $Ba(OH)_2 \cdot 8H_2O$ (0.236 g, 0.75 mmol; Fisher, ACS reagent), NaOH (4 g, 100 mmol; Fisher, ACS reagent). Reagents were placed in a 12.5 mm diameter silver tube that had been sealed at one end and which was crimped at the other end. The silver tube was placed into a box furnace and heated to the reaction temperature of 650°C at 50°C/h, held for 12 h, and then cooled to room temperature by turning off the furnace. The crystals were extracted from the flux matrix by sonication in methanol.

2.3. Magnetic susceptibility

The magnetic susceptibility data for these oxides were obtained using a Quantum Design MPMS XL SQUID magnetometer. For the magnetic measurements, loose crystals of the irradiates were placed into a gelatin capsule, which was placed inside a plastic straw. Samples were measured under both zero-field cooled (ZFC) and field cooled (FC) conditions. In either case the magnetization was measured in the temperature range 5–300 K. Susceptibility measurements were carried out in an applied field of 10 kG.

2.4. Microscopy

Scanning electron micrographs of several single crystals were obtained using a Philips XL 30 ESEM instrument utilized in the environmental mode. For $Ba_{3.44}K_{1.56}Ir_2O_{10}$, EDS verified the presence of barium, potassium, iridium, and oxygen, while for $Ba_3LiIr_2O_9$ and $Ba_3NaIr_2O_9$, EDS verified the presence of barium, sodium, iridium and oxygen. Lithium was not observed as it is below the detection limit of the instrument. No other extraneous elements were detected within the detection limits of the instrument.

2.5. Data collection for $Ba_{3.44}K_{1.56}Ir_2O_{10}$

For the structure determination, a black hexagonal crystal was mounted onto the end of a thin glass fiber. X-ray intensity data were measured at 293 K on a Bruker SMART APEX CCD-based diffractometer system (Mo$K\alpha$ radiation, $\lambda = 0.71073$ Å) [37]. Crystal quality and initial unit cell parameters were determined based on reflections taken from a set of three scans measured in orthogonal regions of reciprocal space. Subsequently, 1.5 hemispheres of frame data were collected with a scan width of 0.3° in ω and an exposure time of 30 s. per frame ($R_{int} = 0.0398$, avg. redundancy = 9.72, $2\theta_{max} = 68.6°$). The first 50 frames were re-collected at the end of data set to monitor crystal decay. The raw data frames were integrated with the Bruker SAINT + program [37], which also applied

Table 1
Crystallographic data for $Ba_3MIr_2O_9$ (M = Li, Na) and $Ba_{3.44}K_{1.56}Ir_2O_{10}$

Formula	$Ba_3LiIr_2O_9$	$Ba_3NaIr_2O_9$	$Ba_{3.44}K_{1.56}Ir_2O_{10}$
Space group	$P6_3/mmc$	$P6_3/mmc$	$P6_3/mmc$
a (Å)	5.7804(4)	5.866(4)	5.9133(1)
c (Å)	14.302(1)	14.596(1)	18.1792(7)
V (Å^3)	413.86(5)	434.94(5)	550.51(2)
Z	2	2	2
Density calculated (g/cm^3)	7.354	7.600	6.502
Crystal size (mm)			$0.12 \times 0.05 \times 0.04$
Diffractometer	Enraf–Noius CCD		Bruker Smart Apex CCD
Radiation		Mo$K\alpha$ ($\lambda = 0.71073$ Å)	
Collection region (2θ limit)	$2.85 \leqslant 2\theta \leqslant 29.96$	$2.79 \leqslant 2\theta \leqslant 39.99$	$2.24 \leqslant 2\theta \leqslant 34.31$
No. of used reflections	242	493	495
No. of variable parameters	22	22	25
R, R_w	0.0198, 0.0486	0.0192, 0.0434	0.0419, 0.0857

corrections for Lorentz and polarization effects. The final unit cell parameters are based on the least-squares refinement of 4230 reflections from the data set with $I > 5\sigma(I)$. Analysis of the data showed negligible crystal decay during data collection. An empirical absorption correction based on the multiple measurement of equivalent reflections was applied with the program SADABS [37]. The structure was solved by a combination of direct methods and difference Fourier syntheses, and refined by full-matrix least-squares against F^2 (SHELX) [38]. Relevant crystallographic information for $Ba_{3.44}K_{1.56}Ir_2O_{10}$ is gathered in Table 1.

2.6. Data collection for $Ba_3LiIr_2O_9$ and $Ba_3NaIr_2O_9$

For the structure determination, black hexagonal crystals were mounted onto the end of a thin glass fiber. The data collection was performed with a Brucker Nonius Kappa CCD diffractometer, running the Collect software package [39] (Mo$K\alpha$ radiation $\lambda = 0.71073$ Å). A preliminary peak search using eight frames was used to determine the unit cell parameters and to ascertain the quality of the chosen crystals. Data were collected up to $\theta_{max} = 30°$ ($Ba_3LiIr_2O_9$) and $\theta_{max} = 40°$ ($Ba_3NaIr_2O_9$) with an exposure time of 30 s and d$x = 30$ mm. The frame images were integrated using the Evald CCD software [39] and absorption corrections were made using the Gaussian method in both cases. The resulting data were sorted and merged with a mean redundancy of 19 ($Ba_3LiIr_2O_9$) and 22 ($Ba_3NaIr_2O_9$) using the program JANA2000. [40] The final unit cell parameters are based on the least-squares refinement of 242 ($Ba_3LiIr_2O_9$) and 493 ($Ba_3NaIr_2O_9$) reflections with $I > 3\sigma(I)$. Analyses of the data showed negligible crystal decay during data collection. The 6h-$BaTiO_3$ positions were used as a starting model and the structures were subsequently refined by full-matrix least-squares against F^2 (JANA2000) [40]. Relevant crystallographic information for the two compounds is gathered in Table 1.

3. Results and discussion

3.1. Crystal structures

3.1.1. $Ba_{3.44}K_{1.56}Ir_2O_{10}$

The structure was solved in the hexagonal space group $P6_3/mmc$ and found to be isostructural with $Ba_5Ru_2O_{10}$ [8], which is an $n = 3$ member of the $[A_nB_{n-1}O_{3n}][A_2O]$ family of structures, consisting of $[AO_3]$ and $[A_2O]$ layers. During the structural refinement, without consideration of potassium incorporation from the flux, an enlarged displacement parameter for Ba in the $[A_2O]$ layers was observed. Refinement of the site occupation factor (sof) for the Ba resulted in a significant decrease from unity, which suggested the partial occupation of another species with a smaller scattering factor than barium in this site.

Refinement of this site as a fully occupied Ba/K mixed site resulted in the final ratio 0.224(7)/0.776(7) (Ba/K). No other metal atom showed evidence of partial occupancy or site mixing, and during the structure solution it was determined that the $[AO_3]$ layers are solely occupied by barium and that the extra potassium was only located in the $[A_2O]$ layer. The overall composition of the crystal was determined to be $Ba_{3.44(1)}K_{1.56(1)}Ir_2O_{10}$. The presence of potassium in $Ba_{3.44(1)}K_{1.56(1)}Ir_2O_{10}$ was established by EDS measurements. Qualitative EDS results measured on several representative crystals gave an average composition of 3.49:1.51 for Ba:K, which is in good agreement with the composition obtained from the single crystal structure determination. The source of the potassium was the KO_2/KOH flux, making it a reactive flux for this system.

The atomic positions for $Ba_{3.44(1)}K_{1.56(1)}Ir_2O_{10}$ are listed in Table 2 and a representation of the structure is shown in Fig. 1. The structure can be described as resulting from the stacking of close packed $[BaO_3]$ sheets according to the sequence $ABAACA$, that is divided by one $[(Ba/K)_2O]$ layer (x) to give the sequence

Table 2
Atomic coordinates and thermal parameters (Å^2) for $Ba_3MIr_2O_9$ (M = Li, Na) and $Ba_{3.44}K_{1.56}Ir_2O_{10}$

	x	y	z	U_{eq}	U_{11}	U_{22}	U_{33}	U_{12}	U_{13}	U_{23}
$Ba_3LiIr_2O_9$										
Ba1	2/3	1/3	0.08653(5)	0.0131(2)	0.0129(3)	0.0129(3)	0.0134(4)	0.0065(1)	0	0
Ba2	0	0	1/4	0.0117(3)	0.0112(3)	0.0112(3)	0.0128(5)	0.0056(2)	0	0
Ir	1/3	2/3	0.15364(3)	0.0086(2)	0.0089(2)	0.0089(2)	0.0080(3)	0.0044(1)	0	0
Li	0	0	0	0.002(6)	0.001(6)	0.001(6)	0.004(12)	0.001(3)	0	0
O1	0.4836(7)	0.5164(7)	1/4	0.012(2)	0.013(2)	0.013(2)	0.013(3)	0.009(3)	0	0
O2	0.1734(5)	0.3469(9)	0.0849(3)	0.013(2)	0.016(2)	0.010(2)	0.012(2)	0.005(1)	−0.0002(11)	0.000(2)
$Ba_3NaIr_2O_9$										
Ba1	2/3	1/3	0.08720(3)	0.0128(1)	0.0103(1)	0.0103(1)	0.0177(2)	0.0052(1)	0	0
Ba2	0	0	1/4	0.0096(1)	0.0080(1)	0.0080(1)	0.0126(2)	0.0040(1)	0	0
Ir	1/3	2/3	0.15664(1)	0.0062(1)	0.0054(1)	0.0054(1)	0.0080(1)	0.0027(1)	0	0
Na	0	0	0	0.0071(7)	0.0065(7)	0.0065(7)	0.008(2)	0.0033(4)	0	0
O1	0.4830(3)	0.5170(3)	1/4	0.010(1)	0.010(1)	0.010(1)	0.014(2)	0.008(1)	0	0
O2	0.1777(3)	0.3554(6)	0.0880(2)	0.0156(8)	0.0166(9)	0.011(1)	0.017(1)	0.0056(6)	−0.0032(6)	−0.006(1)
$Ba_{3.44}K_{1.56}Ir_2O_{10}$										
Ba1	0	0	0.1396(1)	0.013(1)	0.0013(1)	0.0013(1)	0.0012(1)	0.007(1)	0	0
Ba2	1/3	2/3	1/4	0.011(1)	0.007(1)	0.007(1)	0.0019(1)	0.004(1)	0	0
Ba3[a]	1/3	2/3	0.0134(1)	0.0018(1)	0.0021(1)	0.0021(1)	0.0011(1)	0.0010(1)	0	0
K[a]	1/3	2/3	0.0134(1)	0.0018(1)	0.0021(1)	0.0021(1)	0.0011(1)	0.0010(1)	0	0
Ir	2/3	1/3	0.1729(1)	0.008(1)	0.005(1)	0.005(1)	0.0013(1)	0.003(1)	0	0
O1	0.5105(9)	0.022(2)	0.1182(4)	0.0015(2)	0.0014(3)	0.007(3)	0.0021(3)	0.004(2)	−2(2)	−4(3)
O2	0.372(2)	0.186(1)	1/4	0.0010(2)	0.000(4)	0.005(3)	0.0021(5)	0.000(2)	0	0
O3[a]	0.087(6)	0.087(6)	0	0.004(6)						

[a] The site occupation factors (sof) for Ba3 and K are 0.776(7) and 0.224(7), respectively. The sof for O3 was fixed at 1/6.

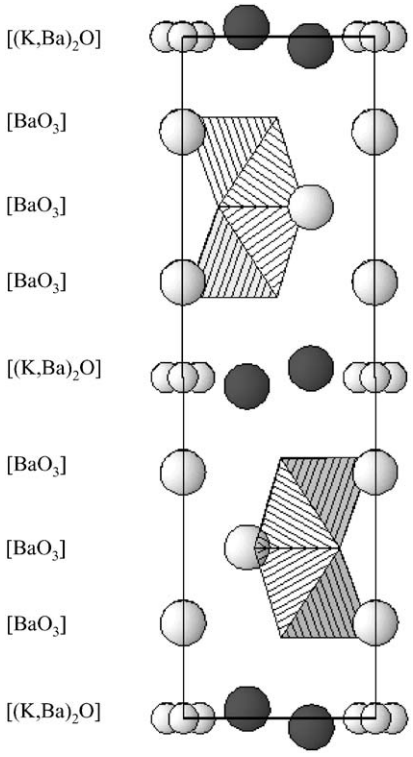

Fig. 1. Representation of the $Ba_{3.44}K_{1.56}Ir_2O_{10}$ structure viewed along the b-axis.

ABAxACA. The [BaO_3] and [(Ba/K)$_2$O] layers are shown schematically in Fig. 2.

The iridium cations occupy the octahedral sites between the [BaO_3] sheets, resulting in the formation of [$Ba_3Ir_2O_9$] slabs separated by one [(Ba/K)$_2$O] layer. Within the [$Ba_3Ir_2O_9$] slabs, the iridium cations form isolated, face-sharing Ir_2O_9 octahedra pairs. The structure is, thus, related to the 6H-perovskite structure, such as $Ba_3NaIr_2O_9$, vide infra, which contains Ir_2O_9 face-sharing octahedra pairs that corner share with isolated NaO_6 octahedra. In the case of $Ba_{3.44}K_{1.56}Ir_2O_{10}$, however, the octahedra pairs are not connected to one another via corner sharing octahedra. The octahedral pairs along the c-direction are physically isolated by the intervening [(Ba/K)$_2$O] layers.

While the oxygen atoms of the Ir_2O_9 bi-octahedron behave normally, oxygen O3 is disordered about a $\bar{3}$ axis. Free refinement of the sof for O3 yielded a value of 1/6. The sof for O3 was subsequently fixed at 1/6, and O3 was refined with an isotropic displacement parameter. Such a disorder of the oxygen atoms in the [A_2O] layer has been previously observed in a structurally related manganate, $La_2Ba_{0.8}Sr_{0.6}Ca_{1.6}Mn_2O_{10}$ [41].

Selected interatomic distances and bond angles for $Ba_{3.44}K_{1.56}Ir_2O_{10}$ are compiled in Table 3. The coordination number of Ba1, Ba2 and Ba3/K atoms are 10, 12

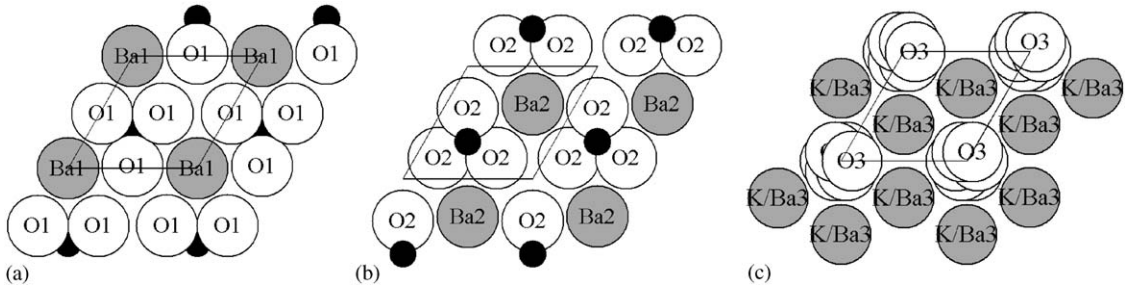

Fig. 2. Representations of $[BaO_3]$ (a) and $[(Ba,K)_2O]$ (b) layers and their stacking mode (c) in $Ba_{3.44}K_{1.56}Ir_2O_{10}$. The small black spheres indicate the adjacent iridium atoms.

Table 3
Selected interatomic distances (Å) for $Ba_3MIr_2O_9$ (M = Li, Na) and $Ba_{3.44}K_{1.56}Ir_2O_{10}$

$Ba_3LiIr_2O_9$			
Ba1–O1 × 3	2.971(3)	Li–O2 × 6	2.119(5)
Ba1–O2 × 6	2.891(4)	Ir–O1 × 3	2.040(4)
Ba1–O2 × 3	2.928(5)	Ir–O2 × 3	1.878(6)
Ba2–O1 × 6	2.895(3)	Ir–Ir	2.7563(6)
Ba2–O2 × 6	2.931(5)		
$Ba_3NaIr_2O_9$			
Ba1–O1 × 3	3.0213(14)	Na–O2 × 6	2.216(3)
Ba1–O2 × 6	2.935(3)	Ir–O1 × 3	2.042(2)
Ba1–O2 × 3	3.007(3)	Ir–O2 × 3	1.872(3)
Ba2–O1 × 6	2.938(2)	Ir–Ir	2.7253(2)
Ba2–O2 × 6	2.975(3)		
$Ba_{3.44}K_{1.56}Ir_2O_{10}$			
Ba1–O1 × 6	2.984(11)	Ir–O1 × 3	1.883(9)
Ba1–O2 × 3	2.768(7)	Ir–O2 × 3	2.059(8)
Ba1–O3 × 1	2.589(7)	Ir–Ir	2.8042(14)
Ba2–O1 × 6	3.005(9)		
Ba2–O2 × 6	2.9634(7)		
Ba3/K–O1 × 3	2.632(9)		
Ba3/K–O1 × 3	2.878(9)		
Ba3/K–O3 × 3	2.99(3)		

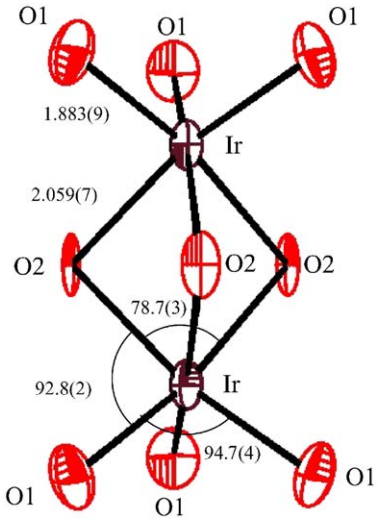

Fig. 3. Structure of the Ir_2O_9 dimer in $Ba_{3.44}K_{1.56}Ir_2O_{10}$—50% probability thermal ellipsoids, selected bond distances (Å) and bond angles (°).

and 9, respectively. The grouping of three short Ir–O distances at 1.883(9) Å and three long at 2.059(8) Å within the Ir_2O_9 bi-octahedra is typical for octahedra pairs in perovskites and perovskite related structures (Fig. 3). Comparable Ir–O distances of 1.872(3) and 2.042(2) Å are found in the triple perovskite $Ba_3NaIr_2O_9$, discussed next. The Ir–Ir distance of 2.804(1) Å in $Ba_{3.44}K_{1.56}Ir_2O_{10}$ is slightly longer than that found for the face-sharing octahedra pair in $Ba_3NaIr_2O_9$, 2.7253(2) Å, which is consistent with the stronger repulsive force on the Ir ions due to the higher average oxidation state of 5.78 in $Ba_{3.44}K_{1.56}Ir_2O_{10}$, compared to 5.5 in $Ba_3NaIr_2O_9$.

Using the crystal growth conditions described for this compounds, it is possible to force high oxidation states onto the metals in the crystals; however, there are chemical limitations as to what the highest achievable oxidation state is for any particular metal. Consequently, in structures where the elemental stoichiometry would force the metal to take on too-high an oxidation state, one often observes oxygen deficient layers that charge compensate and enable the metal to remain in a slightly lower oxidation state [6]. If we think of the $[(Ba/K)_2O]$ layer as a severely oxygen deficient $[AO_3]$ layer, then perhaps its role is to keep the oxidation state of the iridium within chemically acceptable limits, which in this case is the nonetheless unusually high average oxidation state of 5.78.

3.1.2. $Ba_3LiIr_2O_9$ and $Ba_3NaIr_2O_9$

The structures of $Ba_3LiIr_2O_9$ and $Ba_3NaIr_2O_9$ were solved in the hexagonal space group $P6_3/mmc$ and both were found to be isostructural with the 6H–$BaTiO_3$ or triple perovskite structure. The atomic positions are listed in Table 2, selected interatomic distances in Table 3 and the structure of $Ba_3MIr_2O_9$ (M = Li, Na) is shown in Fig. 4. It consists of face-sharing Ir_2O_9 octahedra pairs, which in turn share six vertices to six MO_6 (M = Li, Na) octahedra. In terms of stacking of close packed layers, the triple perovskite is a combination of

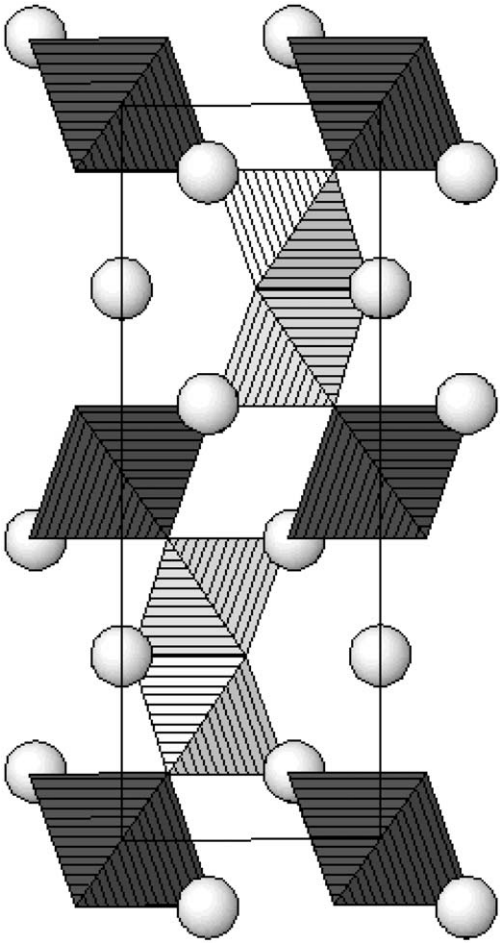

Fig. 4. Representation of the $Ba_3NaIr_2O_9$ structure.

hexagonal (*ABAB*) and cubic (*ABCABC*) stacked [AO_3] layers, creating the face-shared octahedra pairs and the vertex-shared octahedra, respectively. The barium atoms are located in 12-fold coordination sites. The alkali metal to oxygen distances measure 2.119(5) Å for LiO_6 and 2.216(3) Å for NaO_6 and are in good agreement with other M–O distances (M = Li, Na) observed in other triple perovskites, such as $Ba_3MRu_2O_9$ and $Ba_3MOs_2O_9$ (M = Li, Na) [24,42]. As in the structure of $Ba_{3.44}K_{1.56}Ir_2O_{10}$, here also are two different Ir–O distances within the octahedra pair; three long distances measuring 2.040(4) and 2.042(2) Å for the lithium and sodium analogs, respectively, and three short distances of 1.878(6) and 1.872(3) Å for the lithium and sodium analogs, respectively. The existence of short and long metal oxygen distances in the face-sharing octahedra pairs is typical for triple perovskites. The long Ir–O distance is formed by the set of three oxygen that are located in the shared-face of the octahedra pair and the short distance is to the outer set of six oxygen that corner share to the lithium (sodium) containing octahedra. The short Ir–O distances are comparable to the analogous distances in $Ba_{3.44}K_{1.56}Ir_2O_{10}$ (vide supra) and $Ba_3LiIr_2O_9$ and $Ba_3NaIr_2O_9$. The Ir–Ir interatomic distances measure 2.7563(6) and 2.7253(2) Å for the lithium and sodium analogs, respectively, and are in the range expected for iridium in an average oxidation state of 5.5. Gore and Battle have most recently investigated polycrystalline samples of $Ba_4LiIr_3O_{12}$ and $Ba_4NaIr_3O_{12}$ [43], which were also found to form in the 6H-perovskite structure, and which have iridium oxidation states of +5. Due to the mixing of lithium and iridium on the 2a site, it is difficult to make quantitative comparisons between these materials and our fully ordered materials; nonetheless, there is excellent qualitative agreement between the structural parameters.

3.2. Magnetism

The temperature dependence of the magnetic susceptibility for $Ba_{3.44}K_{1.56}Ir_2O_{10}$ in an applied field of 10 kG is shown in Fig. 5a. The susceptibility increases steadily with decreasing temperature and shows no indication of long range order. The ZFC and FC data completely overlay at all temperatures except for a very slight deviation at the very lowest temperatures measured. One would expect strong local antiferromagnetic coupling within the face-sharing Ir_2O_9 octahedra pairs, as has been observed in $Ba_5Ru_2O_{10}$ and $La_2Ba_{0.8}Sr_{0.6}Ca_{1.6}Mn_2O_{10}$.

The inverse susceptibility (Fig. 5a inset) is non-linear up to 300 K, the highest temperature measured, which makes it unreliable for calculating a magnetic moment for this compound. Attempting a fit using the Curie–Weiss Law with a correction for temperature independent paramagnetism (TIP) according to the equation $\chi_m = C/(T-\theta) + \chi_{TIP}$, yielded a Curie constant, $C = 0.825$ emu/mol K, a μ_{eff} of 2.56 μ_B per formula unit, a Weiss temperature, $\theta = -29$ K and a temperature independent paramagnetic term, $\chi_{TIP} = 2.9 \times 10^{-4}$ emu/mol. These values can at best be thought of as ballpark figures, as the susceptibility data does not follow the curie law over any appreciable temperature range. Nonetheless, by comparison, this calculated moment is significant smaller than the theoretical spin-only moment, $\mu_{s.o.}$ calculated for non-interacting mixed valent Ir^{5+}/Ir^{6+}. By using spin-only moments for Ir^{5+} (2.83 μ_B) and Ir^{6+} (3.87 μ_B), one calculates a moment of 5.19 μ_B from the equation

$$\mu_{eff} = \sqrt{0.44\,\mu^2_{s.o.}(Ir^{5+}) + 1.56\,\mu^2_{so}(Ir^{6+})}.$$

Of course, we would expect the observed moment to be smaller than the spin-only value due to the presence of spin–orbit coupling and antiferromagnetic correlations in the octahedra pairs.

We can qualitatively discuss what one might anticipate for the magnetic behavior of $Ba_{3.44}K_{1.56}Ir_2O_{10}$. The iridium cations are located in the face-sharing octahedra

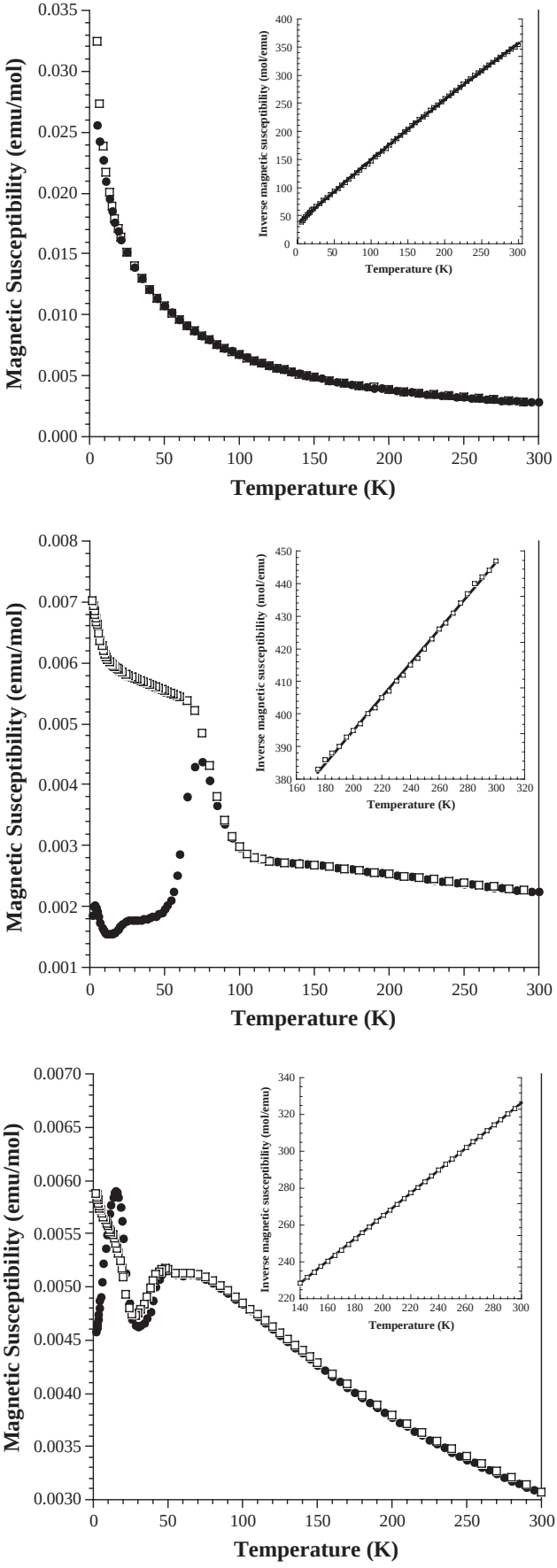

pairs and we expect strong antiferromagnetic exchange interactions to be present. Due to the fact that the iridium in these octahedra pairs is mixed valent, +5 (spin 1) and +6 (spin 3/2), we expect a magnetic ground state and a contribution from higher energy electron configurations with increasing temperature, contributing to the nonlinear inverse susceptibility curve.

For comparison, the magnetic susceptibilities of $Ba_3LiIr_2O_9$ and $Ba_3NaIr_2O_9$ are shown in Figs. 5b and c, respectively. The susceptibilities increases steadily with decreasing temperature and show signs of magnetic order at 75 and 50 K for the lithium and sodium compound, respectively. At these temperatures, the ZFC and FC data diverge, suggesting the presence of magnetic coupling and spin frustration. As in the case of $Ba_{3.44}K_{1.56}Ir_2O_{10}$, one would also expect strong local antiferromagnetic coupling within the face-sharing Ir_2O_9 octahedra pairs. The inverse susceptibility (Figs. 5b and c insets), is fairly linear up to 300 K, the highest temperature measured. A fit using the Curie–Weiss Law, $\chi = C/(T-\theta)$, yielded a Curie constant, $C = 1.965$ emu/mol K, a Weiss temperature, $\theta = -576$ K, and a calculated effective moment of 3.93 emu/mol for $Ba_3LiIr_2O_9$. The magnetic data for $Ba_3LiIr_2O_9$ is in qualitative agreement with what was observed by Gore and Battle for $Ba_4LiIr_3O_{12}$ [43], for which the FC and ZFC data diverge at 56 K (no data are reported for the sodium analog). They did not report a magnetic moment for $Ba_4LiIr_3O_{12}$. The fit of the sodium analogue, $Ba_3NaIr_2O_9$, results in a Curie constant, $C = 1.630$ emu/mol K, a Weiss temperature, $\theta = -232$ K, and a calculated effective moment of 3.60 emu/mol. In both the sodium and the lithium analog, we assume also that the lower magnetic moments are due to a combination of spin–orbit coupling and strong exchange interactions within the Ir_2O_9 octahedra pairs that lower the magnetization of the samples.

If we compare the three compounds, we find that in the case of $Ba_3LiIr_2O_9$ and $Ba_3NaIr_2O_9$, the face-sharing Ir_2O_9 octahedra pairs are connected via LiO_6 and NaO_6 corner sharing octahedra, respectively. This connection can facilitate superexchange interactions that lead to the observed long-range order. By contrast, the Ir_2O_9 octahedra pairs in $Ba_{3.44}K_{1.56}Ir_2O_{10}$ are not connected via corner sharing octahedra and are in fact more isolated due to the intervening $[(Ba/K)_2O]$ layer, which may account for the lack of observed long-range magnetic order.

Fig. 5. Temperature dependence of ZFC (closed circles) and FC (open squares) molar magnetic susceptibilities measured in an applied field of 10 kG for: (a) $Ba_{3.44}K_{1.56}Ir_2O_{10}$ (top), (b) $Ba_3LiIr_2O_9$ (middle), and (c) $Ba_3NaIr_2O_9$ (bottom). Insets: The fits of the inverse susceptibilities are shown.

4. Conclusion

In summary, the use of a hydroxide flux enabled us to prepare single crystals of a new oxide, $Ba_{3.44}K_{1.56}Ir_2O_{10}$, an $n = 3$ member of the $[A_nM_{n-1}O_{3n}][A_2O]$ family of hexagonal perovskite related oxides and two ordered triple perovskites, $Ba_3LiIr_2O_9$ and $Ba_3NaIr_2O_9$. All three oxides have iridium in unusually high oxidations states, which can be achieved under the oxidizing conditions of hydroxide fluxes. The magnetic moments determined from the temperature dependence of the magnetic susceptibility are low for all three oxides and is explained as being due to a combination of spin–orbit coupling and antiferromagnetic Ir–Ir exchange interactions that lower the magnetization of the samples.

Supplementary materials

Further details of the crystal structure investigations can be obtained from the Fachinformationszentrum Karlsruhe, 76344 Eggenstein-Leopoldshafen, Germany, (fax (49) 7247-808-666; email: crysdata@fiz.karlsruhe.ed) on quoting the depository numbers CSD-413452—Ba3 Ir2 Na1 O9; CSD-413453—Ba3 Ir2 Li1 O9; CSD-413454—Ba3.44 Ir2 K1.56 O10.

Acknowledgments

Financial support from the National Science Foundation through Grant DMR: 0134156 is gratefully acknowledged.

References

[1] K.E. Stitzer, J. Darriet, H.-C. zur Loye, Curr. Opin. Solid State Mater. Sci. 5 (2001) 535.
[2] J.J. Lander, Acta Crystallogr. 4 (1951) 148.
[3] A.F. Wells, Structural Inorganic Chemistry, Clarendon Press, New York, 1984.
[4] I.S. Kim, T. Nakamura, M. Itoh, Bull. Chem. Soc. Jpn. 71 (1998) 2247.
[5] P.D. Battle, S.H. Kim, A.V. Powell, J. Solid State Chem. 101 (1992) 161.
[6] K.E. Stitzer, W.R. Gemmill, M.D. Smith, H.-C. zur Loye, J. Solid State Chem. 175 (2003) 39.
[7] J. Darriet, M.A. Subramanian, J. Mater. Chem. 5 (1995) 543.
[8] F. Grasset, M. Zakhour, J. Darriet, J. Alloys Compounds 287 (1999) 25.
[9] K.E. Stitzer, M.D. Smith, H.-C. zur Loye, Solid State Sci. 4 (2002) 311.
[10] J.B. Claridge, R.C. Layland, R.D. Adams, H.-C. zur Loye, Z. Anorganische. Allg. Chem. 623 (1997) 1131.
[11] J.B. Claridge, R.C. Layland, W.H. Henley, H.-C. zur Loye, Chem. Mater. 11 (1999) 1376.
[12] W.H. Henley, J.B. Claridge, P.L. Smallwood, H.-C. zur Loye, J. Cryst. Growth 204 (1999) 122.
[13] K.E. Stitzer, M.D. Smith, J. Darriet, H.-C. zur Loye, Chem. Commun. (2001) 1680.
[14] M.D. Smith, H.-C. zur Loye, Acta Crystallogr. C 57 (2001) 337.
[15] H.-C. zur Loye, R.C. Layland, M.D. Smith, J.B. Claridge, J. Cryst. Growth 211 (2000) 452.
[16] H.-C. zur Loye, K.E. Stitzer, M.D. Smith, A. El Abed, J. Darriet, Inorganic Chem. 40 (2001) 5152h.
[17] M. Zakhour-Nakhl, J.B. Claridge, J. Darriet, F. Weill, H.-C. zur Loye, J.M. Perez-Mato, J. Am. Chem. Soc. 122 (2000) 1618.
[18] D. Elwell, H.J. Scheel, Crystal Growth from High-Temperature Solutions, Academic Press, New York, 1975.
[19] S. Frenzen, H.K. Müller-Buschbaum, Z. Naturforsch., Series B 50b (1995) 581.
[20] M. Neubacher, H.K. Müller-Buschbaum, Z. Anorg. Allg. Chem. 607 (1992) 124.
[21] M.D. Smith, J.K. Stalick, H.-C. zur Loye, Chem. Mater. 11 (1999) 2984.
[22] G. Wehrum, R. Hoppe, Z. Anorg. Allg. Chem. 617 (1992) 45.
[23] B.A. Reisner, A.M. Stacy, J. Am. Chem. Soc. 120 (1998) 9682.
[24] K.E. Stitzer, M.D. Smith, W.R. Gemmill, H.-C. zur Loye, J. Am. Chem. Soc. 124 (2002) 13877.
[25] J.A. Campá, E. Gutiérrez-Puebla, M.A. Monge, I. Rasines, C. Ruíz-Valero, J. Solid State Chem. 108 (1994) 230.
[26] K.E. Stitzer, M.D. Smith, H.-C. zur Loye, J. Alloys Compounds 338 (2002) 104.
[27] J.B. Claridge, R.C. Layland, W.H. Henley, H.-C. zur Loye, Z. Anorg. Allg. Chem. 624 (1998) 1951.
[28] M. Zakhour-Nakhl, J. Darriet, J.B. Claridge, H.-C. zur Loye, J.M. Perez-Mato, Int. J. Inorganic Mater. 2 (2000) 503.
[29] M.J. Davis, M.D. Smith, H.-C. zur Loye, Acta Crystallogr. C 57 (2001) 1234.
[30] M.J. Davis, M.D. Smith, K.E. Stitzer, H.C. zur Loye, J. Alloys Compounds 351 (2003) 95.
[31] G.R. Blake, P.D. Battle, J. Sloan, J.F. Vente, J. Darriet, F. Weill, Chem. Mater. 11 (1999) 1551.
[32] P.D. Battle, G.R. Blake, J. Sloan, J.F. Vente, J. Solid State Chem. 136 (1998) 103.
[33] A.V. Powell, P.D. Battle, J.G. Gore, Acta Crystallogr. C 49 (1993) 852.
[34] N. Segal, J.F. Vente, T.S. Bush, P.D. Battle, J. Mater. Chem. 6 (1996) 395.
[35] J. Darriet, F. Grasset, P.D. Battle, Mater. Res. Bull. 32 (1997) 139.
[36] J.-H. Choy, D.-K. Kim, S.-H. Hwang, G. Demazeau, D.-Y. Jung, J. Am. Chem. Soc. 117 (1995) 8557.
[37] SMART Version 5.624, SAINT+ Version 6.02a and SADABS. Bruker Analytical X-ray Systems, Inc., Madison, Wisconsin, USA, 1998.
[38] G.M. Sheldrick, SHELXTL Version 5.1. Bruker Analytical X-ray Systems, Inc., Madison, Wisconsin, USA, 1997.
[39] KappaCCD Program Package, Nonius BV, Delft, 1998.
[40] V. Petrickec, M. Dusek, Institute of Physics, Praha, Czeck Republic (Jana2000).
[41] L. Bie, J. Lin, Y. Wang, C.-K. Loong, Inorganic Chem. Commun. 5 (2002) 966.
[42] K.E. Stitzer, A. El Abed, M.D. Smith, S.-J. Kim, J. Darriet, H.-C. zur Loye, Inorganic Chem. 42 (2002) 947.
[43] J.G. Gore, P.D. Battle, J. Mater. Chem. 6 (1996) 201.